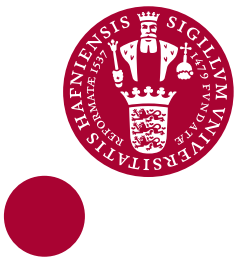

Reaction mechanism of dimethyl ether carbonylation to methyl acetate over mordenite – a combined DFT/experimental study

Rasmussen, D. B.; Chrsitensen, J. M.; Temel, B.; Studt, F.; Moses, P. G.; Rossmeisl, Jan; Riisager, A.; Jensen, A. D.

Published in:
Catalysis Science and Technology

DOI:
10.1039/C6CY01904H

Publication date:
2017

Document version
Peer reviewed version

Reaction mechanism of dimethyl ether carbonylation to methyl acetate over mordenite – a combined DFT/experimental study

D. B. Rasmussen,[a] J. M. Christensen,*[a] B. Temel,[b] F. Studt,[c] P. G. Moses,[b] J. Rossmeisl,[d] A. Riisager[e] and A. D. Jensen*[a]

The reaction mechanism of dimethyl ether carbonylation to methyl acetate over mordenite was studied theoretically with periodic density functional theory calculations including dispersion forces and experimentally in a fixed bed flow reactor at pressures between 10 and 100 bar, dimethyl ether concentrations in CO between 0.2 and 2.0%, and at a temperature of 438 K. The theoretical study showed that the reaction of CO with surface methyl groups, the rate-limiting step, is faster in the eight-membered side pockets than in the twelve-membered main channel of the zeolite; the subsequent reaction of dimethyl ether with surface acetyl to form methyl acetate was demonstrated to occur with low energy barriers in both the side pockets and in the main channel. The present analysis has thus identified a path, where the entire reaction occurs favourably on a single site within the side pocket, in good agreement with previous experimental studies. The experimental study of the reaction kinetics was consistent with the theoretically derived mechanism and in addition revealed that the methyl acetate product inhibits the reaction – possibly by sterically hindering the attack of CO on the methyl groups in the side pockets.

1 Introduction

The global economy and modern society are heavily dependent on a stable price and supply of oil. Currently, most transportation fuel is of fossil origin and its continuous use is thus not sustainable. The unstable prices of fossil fuels and the vulnerability of the global economy to disruption of oil supplies are other factors, which make it evident that the demand for alternative fuels will continue to increase. Ethanol (EtOH) can play an important role in this context as a gasoline additive or substitute.[1–3] Catalytic conversion of syngas (CO/H_2 mixture) to EtOH is an attractive option due to its flexibility with respect to feedstock and potentially high energy efficiency. A number of catalysts for direct conversion of syngas to EtOH have been investigated, but their activity and selectivity towards EtOH are relatively low.[3–14] Recently, an alternative, two-stage process was demonstrated wherein dimethyl ether (DME), which can be formed efficiently and selectively from syngas *via* methanol (MeOH), reacts with CO by carbonylation to form methyl acetate (MA).[15–17] MA is then in a subsequent step hydrogenated to EtOH and MeOH. The main advantage of this indirect process is its unprecedented selectivity towards EtOH, while MeOH, the main by-product, and the unreacted syngas are easily recycled. The challenge that needs to be solved before this process can find industrial application is to increase the activity and stability of the catalyst for MA synthesis.[18] The subsequent hydrogenation of MA to MeOH and EtOH is facile. A number of acidic zeolites are selective catalysts for DME carbonylation and mordenite has the highest activity.[19–21] However, the zeolite catalysts suffer from rapid deactivation due to build-up of coke and large carbonaceous species within the zeolite pores.[21–25] The framework of mordenite contains two types of cavities: eight-membered ring (8-MR) side pockets and 12-MR main channels. It has been reported that MA synthesis takes place in the 8-MR,[26,27] whereas the 12-MR have been suggested to be responsible for the coke formation that leads to catalyst deactivation.[22,25] During the initial phase of DME carbonylation, DME reacts with the Brønsted sites of the zeolite forming surface methyl groups and water [eqn (1) and (2)]:

$$CH_3OCH_3 + [SiO(H)Al] \rightleftharpoons [SiO(CH_3)Al] + CH_3OH \quad (1)$$

$$CH_3OH + [SiO(H)Al] \rightleftharpoons [SiO(CH_3)Al] + H_2O \quad (2)$$

[a] *Department of Chemical and Biochemical Engineering, Technical University of Denmark, Building 229, 2800 Kgs. Lyngby, Denmark. E-mail: jmc@kt.dtu.dk, aj@kt.dtu.dk*
[b] *Haldor Topsøe A/S, Haldor Topsøes Allé 1, DK-2800 Kgs. Lyngby, Denmark*
[c] *SUNCAT Center for Interface Science and Catalysis, SLAC National Accelerator Laboratory, 2575 Sand Hill Road, Menlo Park, CA 94025, USA*
[d] *Department of Physics, Technical University of Denmark, Building 307, 2800 Kgs. Lyngby, Denmark*
[e] *Centre for Catalysis and Sustainable Chemistry, Department of Chemistry, Technical University of Denmark, Building 207, 2800 Kgs. Lyngby, Denmark*

These reactions, in which the Brønsted acid sites are methylated, give rise to an induction period, in which the coverage of methyl groups is building up, and steady-state is reached when the zeolite is fully methylated. The steady-state phase involves the reaction of CO with the methyl groups, forming surface acetyl species, which in turn react with DME, to produce MA and regenerate the methyl groups [eqn (3) and (4)]:

$$CO + [SiO(CH_3)Al] \rightarrow [SiO(CH_3CO)Al] \quad (3)$$

$$CH_3OCH_3 + [SiO(CH_3CO)Al] \rightarrow [SiO(CH_3)Al] + CH_3COOCH_3 \quad (4)$$

Previous experimental studies have shown that formation of the acetyl species [eqn (3)] is the rate-limiting reaction step; the subsequent reaction between DME and acetyl is comparatively fast.[19,20] Also, the reaction kinetics were studied at differential conditions for pressures up to 12 bar, and the reaction was observed to be 1st order in CO and 0th order in DME.[19,20] The previous theoretical studies employing cluster models showed that the reaction of CO with methyl groups is faster in the side pockets than in the main channel, in good agreement with the experimental results. However, it remains to be demonstrated that the reaction of DME with acetyl [eqn (4)] in the side pockets is faster than the reaction of CO with methyl [eqn (3)].[28,29] This is necessary to complete a theoretical explanation of the experimentally observed preference for carbonylation in the 8-MR.

In this study, we investigate the induction and the steady-state phase of DME carbonylation over mordenite in the main channel and in the side pockets, using periodic DFT calculations including the dispersion forces. Additionally, we study the reaction kinetics at high pressures, between 10 and 100 bar, DME concentrations in CO between 0.2 and 2.0%, and at a temperature of 438 K. The insights obtained from the theoretical and experimental studies are then used to develop a kinetic model describing the DME carbonylation.

2 Methods

2.1 DFT calculations

All DFT calculations in this study were performed, using the grid-based, projector augmented wave, DFT program GPAW[30,31] and the ASE program package.[32] Periodic boundary conditions were used for all systems except the molecules in vacuum. A grid spacing of less than 0.18 Å was used for all calculations unless otherwise stated. The reciprocal space was sampled by a (1,1,2)-mesh of Monkhorst–Pack *k*-points.[33] The convergence criteria for the integral of the absolute density change and the integral of the square of the residuals of the Kohn–Sham equations in the self-consistent field were 1.0×10^{-5} electrons and 1.0×10^{-9} eV^2 per electron, respectively. The exchange-correlation energy and potential were calculated within the generalized gradient approximation with the BEEF-vdW functional.[34] The electronic temperatures of 0.1 and 0.0 eV were used for the periodic and non-periodic calculations, respectively.

The unit cell parameters of silicate mordenite were calculated by energy minimization of the optimized structures with respect to the unit cell parameters. These calculations employed a grid spacing of 0.10 Å. The calculated unit cell parameters (a = 18.323 Å, b = 20.795 Å, c = 7.626 Å) compare very well with the experimental values (a = 18.094 Å, b = 20.516 Å, c = 7.542 Å).[35] The framework of mordenite contains 2 types of cavities: 1) eight-membered ring (8-MR) side pockets, parallel to the b axis and 2) 12-MR main channels, parallel to the a axis. The acidic form of mordenite was created by replacing a single Si atom in the silicate unit cell with Al. The unit cell parameters of silicate mordenite were used in all calculations.

The calculations involving molecules in vacuum employed supercells with a vacuum layer of 5.0 Å around the molecule. All systems were optimized using the Broyden–Fletcher–Goldfarb–Shanno (BFGS) algorithm.[36–39] The localization of the transition states and the calculation of the energy barriers were performed using the climbing-image nudged elastic band method.[40] The minimum energy paths were relaxed using the fast inertial relaxation engine (FIRE) and the saddle points were verified by vibrational frequency analysis using a displacement of 0.02 Å.[41] The structures and reaction paths were optimized until the residual force, acting on the atoms, was below 0.03 eV Å^{-1}. The Gibbs free energies are calculated using standard formulas from statistical thermodynamics and assuming harmonic limit for entropy calculations (see Table 5 in Appendix C for the frequencies used for the calculations).[42]

2.2 Experimental details

Mordenite (SiO_2/Al_2O_3 = 20) was obtained from Zeolyst (CBV21A) and all Al sites (1.43×10^{-3} (mol Al) g^{-1}) were used for calculation of the turnover frequencies. The initial ammonium form was converted to the acidic form by heating it at 773 K for 3 h (heating rate 1 K min^{-1}) in a flow of dry air. Before the experiments the catalyst (0.15–1.50 g, 125–250 μm) was calcined in the reactor at 773 K in a flow (200 N ml min^{-1} g^{-1}) of 10 vol% O_2 in N_2 for 3 h (heating rate 1 K min^{-1}) and cooled to the reaction temperature. The experiments were conducted in a high-pressure, fixed-bed flow reactor in which the catalyst was loaded in a quartz tube (OD 10 mm, ID 8 mm) inside a pressure shell.[12] The carbonylation reaction was performed using 2 vol% DME in CO (AGA) diluted to the required DME concentration with CO (AGA), at a flow of 300 Nml min^{-1} and 438 K. The reactor effluent was transferred by heated lines to a mass spectrometer (Hiden Analytical QGA) and to a gas chromatograph (Agilent Technologies, model 6890N) equipped with a DB1 column connected to flame-ionization detector and a Porapak N column, followed by a 13× Molesieve column, connected to a thermal conductivity detector.

3 Results and discussion

3.1 DFT study of the reaction path

There are 4 nonequivalent tetrahedral sites in the unit cell of mordenite: T1 in the 12-MR, T2 and T4 at the intersection between the 12-MR and 8-MR, and T3 in the 8-MR. Because only the T1 and T3 sites are located solely within the 12-MR or 8-MR, respectively, they are considered representative of the main channel and the side pocket. Consequently, all DFT calculations in this study are only performed on the T1 and T3 sites. Table 1 shows the calculated energies of the protons and methyl groups on the T1 and T3 sites of mordenite, which are a measure of their stability. The optimized structures of the methyl groups are shown in Fig. 1.

The protons are almost equally stable on the T1 sites with T1-O4 being only 0.03 eV more energetically favorable than T1-O1. On the T3 sites the preferred adsorption site is clearly T3-O3, which is more stable than T3-O8 (0.19 eV) and T3-O9 (0.17 eV). A similar trend in adsorption strength is observed for methyl groups: T1-O4 and T3-O3 are the favored adsorption sites, more stable than the other sites by at least 0.12 eV.

During the induction phase of the MA synthesis, the Brønsted acid sites react with DME and MeOH, and are, as a result, substituted with methyl groups. Molecules which adsorb on the Brønsted acid sites more strongly than DME or MeOH, without being decomposed, can potentially inhibit the initiation phase. To investigate this effect, we have calculated the adsorption energies of the molecules typically found in the effluent gas during DME carbonylation, on the Brønsted acid sites on T1-O4 and T3-O3 (Table 2). The adsorption energies of ammonia are also included, as they give a measure of the acidity of the proton. The optimized structures of the adsorbed molecules are shown in Fig. 2.

Table 1 Calculated energy of the protons and methyl groups in the main channel on the T1 site and in the side pocket on the T3 site of mordenite. The energies are relative to the most stable proton or methyl group on the same site

H–Z				CH_3–Z			
Position	E (eV)	Position	E (eV)	Position	E (eV)	Position	E (eV)
T1-O1	0.03	T3-O3	0.00	T1-O1	0.12	T3-O3	0.00
T1-O4	0.00	T3-O8	0.19	T1-O4	0.00	T3-O8	0.12
		T3-O9	0.17			T3-O9	0.49

Table 2 Calculated adsorption energies of DME, MeOH, MA, H_2O, AcOH, and NH_3 on a proton in the main channel on the T1-O4 site and in the side pocket on the T3-O3 site of mordenite. The energies are relative to the Brønsted acid site and the molecule in vacuum

	T1 H-O4	T3 H-O3
Species	E_{ads} (eV)	E_{ads} (eV)
NH_3	−1.37	−1.47
MA	−1.12	−1.01
DME	−0.98	−0.99
MeOH	−0.89	−1.09
AcOH	−1.05	−0.90
H_2O	−0.74	−0.87

Ammonia is, as expected from its basic nature, the molecule that adsorbs most strongly on the Brønsted acid sites (as an ammonium cation) and it is 0.10 eV more stable on T3-O3 than on T1-O4. This result shows that the proton is more acidic in the side pocket than in the main channel, which is in good agreement with the experimental results.[26,43,44] The other molecules adsorb in geometries where the oxygen atom in the molecule forms a hydrogen bond with the acidic proton and the molecule is oriented in a manner that leads to additional, weaker, hydrogen bonds between the hydrogen atoms in the molecule and the oxygen atoms in the mordenite framework. AcOH (acetic acid) and MA always adsorb most strongly through the oxygen atom in the carbonyl group. In the main channel, MA and AcOH adsorb more strongly than DME (by 0.14 or 0.07 eV) and MeOH (by 0.23 or 0.16 eV), so both species (especially MA) can potentially inhibit the initiation phase through blockage of the Brønsted acid sites. In the side pocket, MA adsorbs with a similar strength as DME (0.02 eV difference), but weaker than MeOH (0.08 eV). Consequently, MA may inhibit the formation of methyl groups from DME in the side pocket; the inhibition of the path starting from MeOH will likely be less severe. The adsorption energy of AcOH in the side pocket is lower than that of DME and MeOH by 0.09 and 0.19 eV, respectively. AcOH is therefore less likely than MA to inhibit the formation of methyl groups from DME; the formation of methyl groups from MeOH is not expected to be affected. Water is the molecule that adsorbs least strongly and should therefore not be able to block the Brønsted acid sites. However, we have only investigated single-molecule adsorption, and clusters of water molecules may be significantly more stable. This

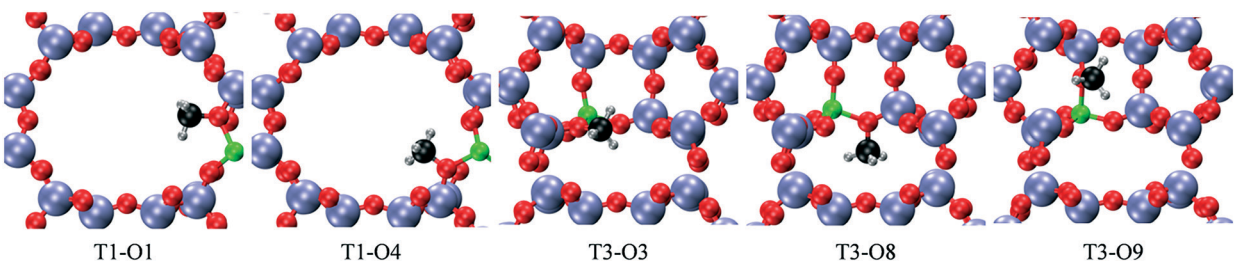

Fig. 1 The optimized structures of the methyl groups in the main channel on the T1 site and in the side pocket on the T3 site of mordenite. O red, Si blue, H gray, C black, Al green.

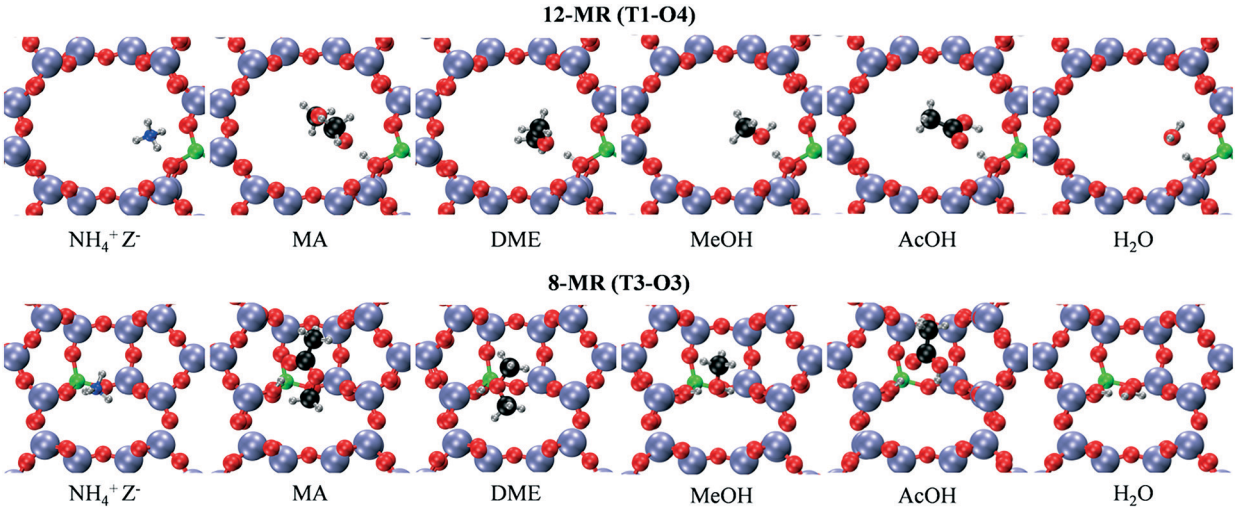

Fig. 2 The optimized structures of the molecules typically found in the effluent gas during DME carbonylation on the Brønsted acid sites within the 12-MR on T1-O4 and the 8-MR on T3-O3 on mordenite. N dark blue, other colors as described in Fig. 1.

effect would be especially important in the side pockets, which have been shown experimentally to be the preferential location of water clusters.[45]

To investigate the reaction path for MA synthesis, we have calculated the activation and reaction energies for the reactions [eqn (1) to (4)], as shown in Table 3. During the induction period the formation of the methyl groups in the main channel is faster from MeOH than from DME (0.07 eV lower energy barrier), whereas both paths are equally active in the side pocket (0.01 eV difference in activation energies). The energy barriers for the reactions of DME and MeOH with a Brønsted acid site are lower in the side pocket than in the main channel by 0.25 and 0.17 eV, respectively, showing that the initiation reactions are significantly faster in the side pocket. Both DME and MeOH are protonated on the oxygen atom during the reaction with the acid proton and the transition states involve a transfer of a methyl group from the protonated intermediate to the zeolite (Fig. 3). The initiation phase of the MA synthesis ends when all Brønsted acid sites have reacted to methyl groups.

Table 3 Calculated activation E_{act} and reaction ΔE energies (eV) for reactions [eqn (1) to (4)] within the 12-MR on T1-O4 and the 8-MR on T3-O3 on mordenite

	T1-O4	T3-O3		
Reaction	E_{act}	ΔE	E_{act}	ΔE
DME + H–Z → MeOH + CH_3–Z	0.62	0.02	0.37	0.01
MeOH + H–Z → H_2O + CH_3–Z	0.55	−0.18	0.38	−0.19
CO + CH_3–Z → CH_3CO^+ + Z^-	1.09	−0.09	1.03	−0.48
CH_3CO^+ + Z^- → CH_3CO–Z	0.02	−0.81	0.01	−0.53
DME + CH_3CO–Z → CH_3–MA^+ + Z^-	0.00	−0.24	0.24	0.13
CH_3–MA^+ + Z^- → MA + CH_3–Z	0.58	−0.24	0.88	−0.48
MeOH + CH_3CO–Z → MA + H–Z	0.00	−0.50	0.02	−0.38
DME + CH_3–Z → TMO^+ + Z^-	0.36	−0.03	0.70	−0.09
H_2O + CH_3CO–Z → AcOH + H–Z	0.06	−0.36	0.20	−0.24

In the further reaction towards MA, a methyl group reacts with CO to form an acetyl carbocation, CH_3CO^+ (Fig. 4). This is the rate-limiting reaction step and the energy barrier for it is 0.06 eV lower in the side pocket than in the main channel. The optimized geometries of the reaction steps and transition states are shown in Fig. 5 (T1-O4) and Fig. 6 (T3-O3). Next, the acetyl carbocation is restructured to acetyl with a very low energy barrier (T1-O4: 0.02 eV, T3-O3: 0.01 eV). As we reported in a recent study, the acetyl carbocation can alternatively react to ketene with higher activation energies (T1-O4: 0.09 eV, T3-O3: 0.12 eV), and the experimental

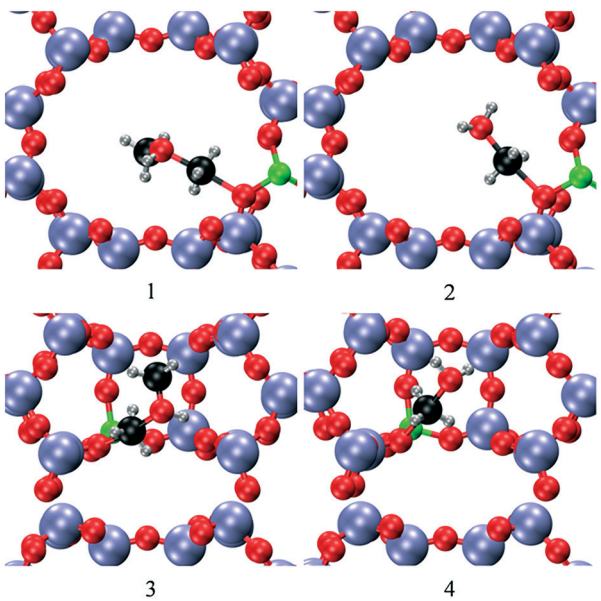

Fig. 3 Optimized structures of the transition states for the reaction of: 1) DME with a Brønsted acid site within the 12-MR on T1-O4 on mordenite, 2) MeOH with a Brønsted acid site within the 12-MR on T1-O4 on mordenite, 3) DME with a Brønsted acid site within the 8-MR on T3-O3 on mordenite, 4) MeOH with a Brønsted acid site within the 8-MR on T3-O3 on mordenite.

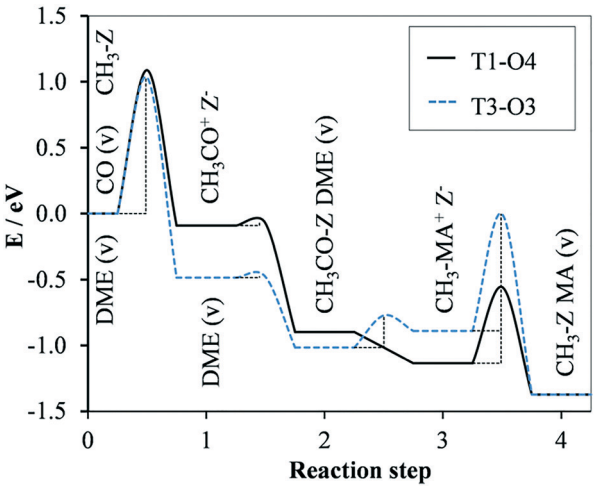

Fig. 4 Reaction paths for formation of MA within the 12-MR on T1-O4 and the 8-MR on T3-O3 on mordenite. Reaction steps: 0: CO and DME in vacuum, methyl group on the zeolite; 1: acetyl carbocation, DME in vacuum and negatively charged zeolite; 2: acetyl group on zeolite, DME in vacuum; 3: CH_3–MA cation and negatively charged zeolite; 4: MA in vacuum, methyl group on zeolite. Full line: reaction steps in the main channel (T1-O4); dotted line: reaction steps in the side pocket (T3-O3).

observation of ketene supported the theoretical model.[46] Ketene is then restructured to acetyl – the energy barriers for this step are (not shown in Table 3) 0.18 eV on T1-O4 and 0.12 eV on T3-O3. The surface acetyl reacts with DME, forming a cationic CH_3–MA^+ complex, which subsequently decomposes to MA in the gas phase leaving a methyl group on the zeolite. The formation of the CH_3–MA^+ complex occurs with no energy barrier in the main channel. The activation energy for this step is 0.24 eV in the side pockets. The transfer of the methyl group from the CH_3–MA^+ complex to the zeolite proceeds with higher energy barriers (T1-O4: 0.58 eV, T3-O3: 0.88 eV) than the formation of the complex (T1-O4: 0.00 eV, T3-O3: 0.24 eV).

Under realistic experimental conditions some MeOH is always present in the system (due to traces of water in the feed and/or due to water formation from coke deposition) and for this reason we have also investigated the reaction between MeOH and the surface acetyl groups. This reaction occurs with no energy barrier in the main channel and with a very low (0.02 eV) energy barrier in the side pocket. This result shows that if MeOH is present in the system it will react very rapidly with the acetyl groups (much faster than DME), forming MA and a Brønsted acid site.

Two other reactions, which may play a role during DME carbonylation over mordenite, are the formation of trimethyloxonium (TMO) species and AcOH. The energy barriers for the reaction of methyl groups with DME are 0.36 and 0.70 eV on T1-O4 and T3-O3, respectively – much lower than for the reactions of methyl groups with CO (T1-O4: 1.09 eV, T3-O3: 1.03 eV). Thus, TMO is formed much faster than acetyl carbocations (which react to acetyl). However, unlike acetyl, TMO is not very stable – the formation energies on T1-O4 and T3-O3 are −0.03 and −0.09 eV, respectively. Consequently, TMO is probably not sufficiently stable to block the T1-O4 and T3-O3 sites, unless it rapidly reacts further to other, more stable species, such as hydrocarbons. This hypothesis is supported by the 0th order DME dependence observed in kinetic studies.[19,20] The energy barriers for the

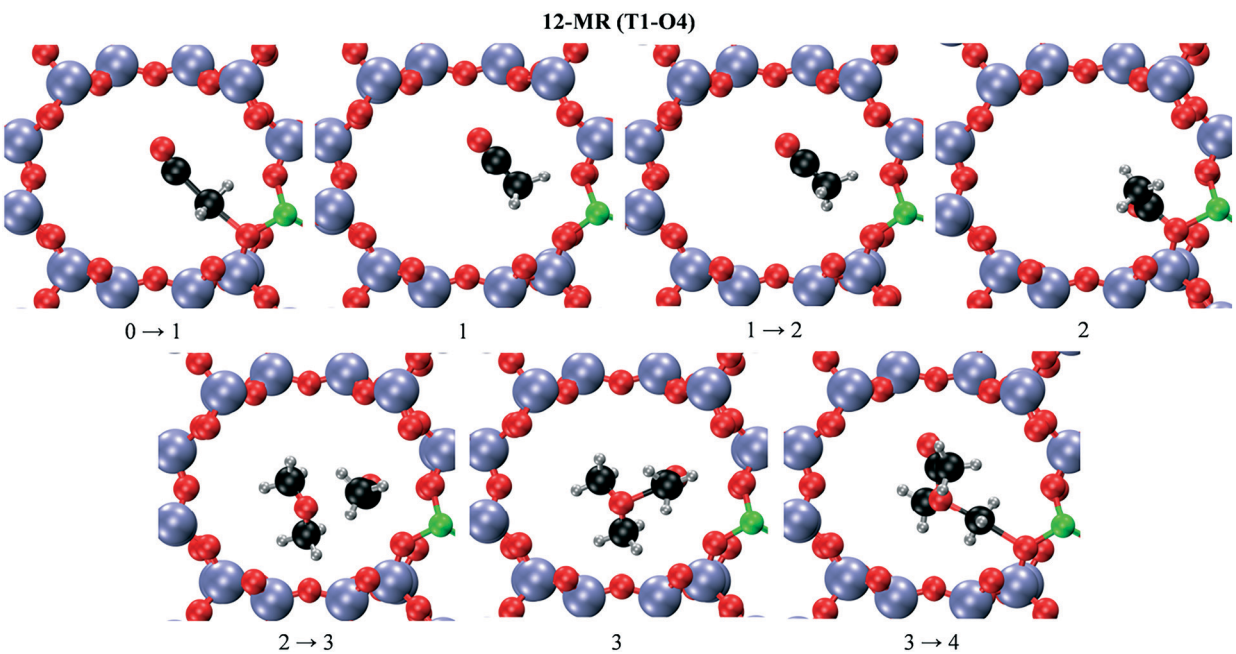

Fig. 5 The optimized structures of the reaction intermediates and transition states for formation of MA within the 12-MR on T1-O4 on mordenite. Reaction steps: 0: CO and DME in vacuum, methyl group on the zeolite; 1: acetyl carbocation, DME in vacuum and negatively charged zeolite; 2: acetyl group on zeolite, DME in vacuum; 3: CH_3–MA cation and negatively charged zeolite; 4: MA in vacuum, methyl group on zeolite.

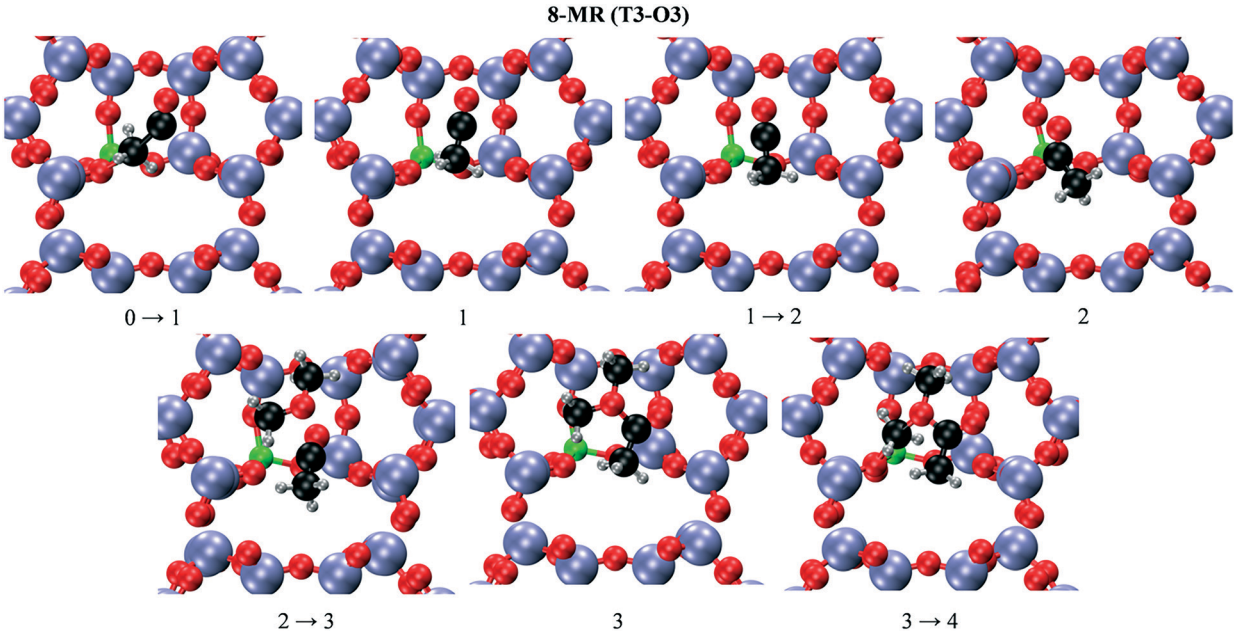

Fig. 6 The optimized structures of the reaction intermediates and transition states for formation of MA within the 8-MR on T3-O3 on mordenite. Reaction steps: 0: CO and DME in vacuum, methyl group on the zeolite; 1: acetyl carbocation, DME in vacuum and negatively charged zeolite; 2: acetyl group on zeolite, DME in vacuum; 3: CH_3–MA cation and negatively charged zeolite; 4: MA in vacuum, methyl group on zeolite.

reaction of acetyl with water (T1-O4: 0.06 eV, T3-O3: 0.20 eV) are lower than for the reaction with DME (T1-O4: 0.58 eV, T3-O3: 0.88 eV). This result shows that if any water is present in the system, acetic acid will be the main product instead of MA.

Our DFT calculations show that the attack of CO on a methyl group, the rate-limiting reaction step, is more facile in the side pocket than in the main channel (the 0.06 eV difference in barriers translates into a factor of about 5 on the rates at 438 K). This is in good agreement with previous experimental and theoretical studies.[26–29] Also, we see that the energy difference of 0.06 eV in barriers, compares very well with adsorption energy of ammonia being 0.10 eV larger in the side pocket than in the main channel. This is in agreement with the proposal that the adsorption energy of ammonia is a good reactivity descriptor in solid acid catalysis.[47–49] Additionally, we show that the reaction of DME with acetyl is significantly faster than the attack of CO on a methyl group, both in the main channel and the side pocket, which is in good agreement with the experimental results.[19,20] In an earlier DFT study,[29] it was shown that the reaction between acetyl and DME does not occur in a number of geometries, where one of the species is in the side pocket and the other in the 8-MR channel below the side pocket. In our study, we present a reaction path, in which acetyl is formed from a methyl group on the T3-O3 site (Fig. 6) – this results in an adsorption geometry of acetyl that enables it to react with DME within the side pocket. This new reaction path occurs with significantly lower activation energy than the paths investigated in the previous theoretical studies (1.0 eV *vs.* 2.2 eV).[29] Additionally, the reaction path presented here occurs preferentially entirely inside the 8-MR side pocket facilitated by the stronger acid sites located there (such as T3-O3) and thus offers a possible explanation of the experimentally observed[26] importance of the sites in the 8-MR.

3.2 Experimental study of the reaction path

The DFT study of the reaction mechanism (section 3.1) has shown that the carbonylation of the surface methyl groups is the rate-limiting reaction step and the reaction rate is higher in the side pockets; the subsequent reaction of the formed surface acetyl with DME is comparatively fast. Additionally, the theoretical studies also suggested that MA can potentially block the Brønsted acid sites in the main channel, and to a lesser extent in the side pockets. To supplement the theoretical results we have also conducted experimental studies of the carbonylation reaction with the aim of investigating, if there are phenomena not accounted for by our theoretical model.

Fig. 7 shows the rate of MA synthesis at a fixed total pressure of 10 bar and various DME concentrations in CO. The reaction rate is constant (0.68 mol (mol Al)$^{-1}$ h^{-1}) for DME concentrations between 0.5 vol% (33% DME conversion) and 2 vol% (9% DME conversion). These results show that the rate of MA synthesis does not depend on the DME pressure even at a value as low as 0.0335 bar (outlet pressure with 0.5 vol% DME in feed). This is in good agreement with the theoretical study as eqn (3) (which does not involve DME) is found to be rate limiting and with previous experimental studies[19,20] reporting a 0th order dependence on DME. At the lowest DME concentration of 0.15 vol% (85% DME conversion) the reaction rate decreases by 19% to a value of 0.55 mol (mol Al)$^{-1}$ h^{-1}. At this high DME conversion, the DME pressure becomes very low towards the end of the catalyst bed (0.00225 bar), and eqn (4) begins to exert a limitation on

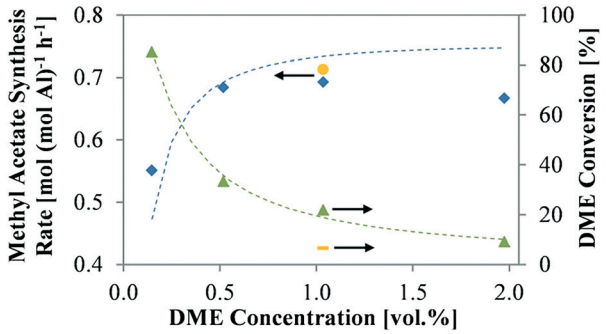

Fig. 7 MA synthesis rate and DME conversion as functions of feed DME concentration in CO at a total pressure of 10 bar: (●) measured MA synthesis rate, 1.5 g catalyst; (▲) measured DME conversion, 1.5 g catalyst; (●) measured MA synthesis rate, 0.5 g catalyst; (–) measured DME conversion, 0.5 g catalyst. Dashed lines are the kinetic model in [eqn (8)].

the rate. Under these conditions, the rate of MA synthesis begins to show a dependence on the DME pressure.

For a fixed composition of the reaction mixture (2 vol% DME in CO), the rate of MA synthesis increases with increasing total pressure (Fig. 8). However, the relationship is not linear as would be expected from the kinetics proposed in the literature.[19,20] The measured reaction rates should lie on a straight line as the reaction is first order in the CO pressure and does not depend on the DME pressure under these conditions. Also, it has been confirmed that the measured reaction rates were not limited by diffusion (Appendix A). A possible explanation is the existence of product inhibition by formed MA, which was found theoretically to bind strongly at Brønsted acid sites (Table 2). To test this we performed two experiments with a reduced catalyst amount (and hence lower product concentration). In the experiment performed at 10 bar and 1 vol% DME in CO (Fig. 7), the catalyst mass was decreased to 1/3 but the TOF per Al atom remained unchanged (<3% change) indicating no product inhibition at this pressure. In the experiment at 100 bar and 2 vol% DME in CO (Fig. 8) the catalyst mass was decreased to 1/10 whereby the TOF per Al atom increased by 39% indicating

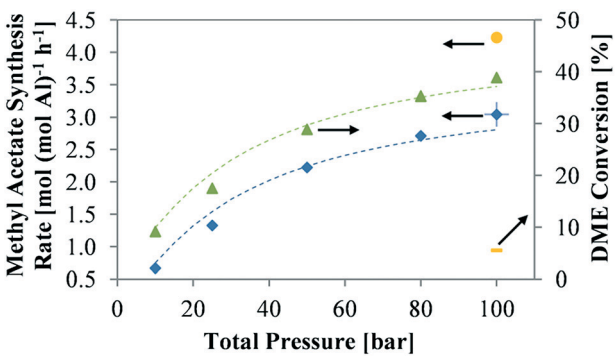

Fig. 8 MA synthesis rate as a function of total reaction pressure (2 vol% DME in CO): (♦) measured MA synthesis rate, 1.5 g catalyst; (▲) measured DME conversion, 1.5 g catalyst; (●) measured MA synthesis rate, 0.15 g catalyst; (–) measured DME conversion, 0.15 g catalyst. (+) measured MA synthesis rate (100 bar, 1.1 vol% DME in CO, 1.5 g catalyst). Dashed lines are calculated from the kinetic model [eqn (11)].

product inhibition at this pressure. These results indicate that MA synthesis is inhibited by the reaction product if the partial pressure of MA is sufficiently high. Further support for this can be found in Fig. 9, which shows how the deviation from the 1st order behavior expected on the basis of measurements of the rate at differential conditions correlates with the average MA pressure in the catalyst bed.[19,20]

To further examine the nature of the MA inhibition, we performed an experiment at 100 bar in which the concentration of DME in CO was reduced from 2 to 1 vol% (Fig. 8). Despite the reduction of the DME pressure in the system, the reaction rate remained the same showing that MA does not react with acetyl; a reaction, in which MA would compete with DME and the reaction rate would depend on the DME pressure. Thus, it seems likely that MA suppresses the reaction by blocking the methyl groups.

Our DFT model shows (Fig. 4) that the formation of the cationic CH_3–MA complexes from a methyl group and a MA molecule in vacuum is endothermic both in the main channel (0.24 eV) and in the side pocket (0.48 eV). Consequently, the CH_3–MA species are not very stable and cannot explain the detrimental effect of MA on the reaction rate. However, MA binds to protonated sites with sufficient strength to inhibit methylation (Table 2), and this may lead to hampering of re-methylation at sites where water (from *e.g.* coke formation) has restored the protonated site. MA at such sites close to the

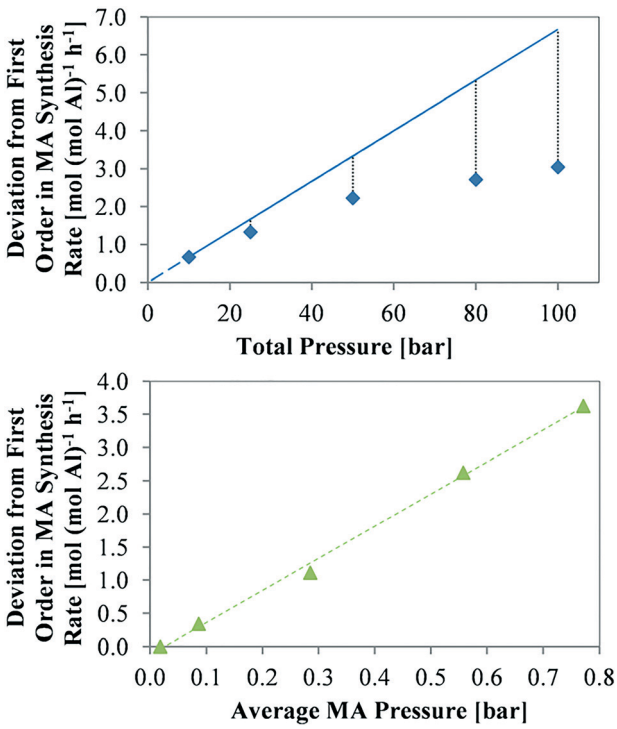

Fig. 9 Top: The deviation from 1st order behavior as a function of total reaction pressure (2 vol% DME in CO, 1.5 g catalyst); the dashed line is the expected 1st order pressure dependence of the MA synthesis rate. Dotted lines indicate deviation from 1st order behaviour. Bottom: The deviation from 1st order behaviour (marked by dotted lines in the top figure) as a function of the average MA pressure in the catalyst bed.

opening of the 8-MR could also block access to the side pockets, rendering the methyl groups inside inactive. Currently, the exact nature of the inhibition remains equivocal, but, as discussed above, likely involves MA sterically hindering the attack of CO on the methyl groups in the side pockets.

Interestingly, it appears from results in the patent literature that this blockage effect also hampers the reactions leading to deactivation (primarily carbon deposition) of the zeolite and can be used to extend the life of the catalyst.[50]

3.3 Kinetic model of the steady-state reaction phase

To describe the state of the catalyst under experimental conditions in steady-state (after the initiation phase), we have developed a kinetic model based on the experimental data in section 3.2 (see Appendix B for the definition of the steady-state). Our DFT calculations show that the activation energies for the carbonylation of the methyl groups are significantly lower than the energy barriers for the reverse reaction (>0.9 eV difference, Table 3). Consequently, we assume an irreversible reaction of CO with a methyl group, in which acetyl is formed [eqn (5)]. The irreversibility of the reaction of CO with a methyl group has also been shown experimentally in previous studies.[19,20]

$$CO + CH_3{-}Z \xrightarrow{k_1} CH_3CO{-}Z \tag{5}$$

The methyl group can be blocked by MA in a quasi-equilibrated reaction forming an inactive complex, here denoted C:

$$MA + CH_3{-}Z \overset{K_2}{\Leftrightarrow} C{-}Z \tag{6}$$

Acetyl reacts with DME, in a quasi-equilibrated reaction, forming MA and regenerating the methyl group:

$$DME + CH_3CO{-}Z \overset{K_3}{\Leftrightarrow} MA + CH_3{-}Z \tag{7}$$

The elementary reactions [eqn (5) to (7)], the quasi-equilibrium assumption for the reactions [eqn (6) and (7)], and a steady-state assumption lead to the following expressions for coverage of the surface species:

$$\Theta_{CH_3} = \frac{1}{1 + K_2 \cdot p_{MA} + K_3^{-1} \cdot \frac{p_{MA}}{p_{DME}}} \tag{8}$$

$$\Theta_C = K_2 \cdot p_{MA} \cdot \Theta_{CH_3} \tag{9}$$

$$\Theta_{Acetyl} = K_3^{-1} \cdot \frac{p_{MA}}{p_{DME}} \cdot \Theta_{CH_3} \tag{10}$$

and the rate expression for the MA synthesis rate:

$$r_{MA} = \frac{k_1 p_{CO}}{1 + K_2 p_{MA} + K_3^{-1} \frac{p_{MA}}{p_{DME}}} \tag{11}$$

The rate expression [eqn (11)] shows that the reaction rate is first order with respect to the pressure of CO. The first term describing the MA inhibition is proportional to the MA pressure and the equilibrium constant for reaction [eqn (6)]. The second MA-inhibition term is proportional to the MA pressure and inversely proportional to the DME pressure. Thus, it will become prominent at high MA pressures and high $\frac{p_{MA}}{p_{DME}}$ ratios; which is the case at high DME conversions.

We determine the parameters k_1, K_2, and K_3 in the kinetic model by modeling the catalyst system as a plug flow reactor, assuming no pressure drop in the catalyst bed, with the design equation:

$$W = F_{DME\_0} \cdot \int_0^X \frac{1}{-r_{DME}} dX \tag{12}$$

where F_{DME_0} is the molar flow of DME at the reactor inlet, X is the conversion of DME at the reactor outlet, r_{DME} is the rate of DME consumption, which equal the rate of MA synthesis (r_{MA}), and W is the mass of the catalyst. The parameters in the kinetic model are determined by fitting eqn (12) to the experimental data using non-linear least squares regression, see Table 4. Fig. 7 and 8 show the rates of MA synthesis and the conversion degrees of DME, as measured experimentally and as calculated using the kinetic model. As seen in Fig. 7 and 8 the developed kinetic model provides a good description of the experimental data.

To obtain information on the state of the catalyst surface under experimental conditions we have calculated the coverage of the surface species as a function of the catalyst mass passed on the way through the bed in a plug flow reactor at 10 and 100 bar (Fig. 10). This is done using the kinetic model for a feed composition of 2 vol% DME in CO. At the total pressure of 10 bar, methyl, acetyl, and CH_3–MA cover 87, 5 and 8% of the catalyst surface, respectively, at the reactor outlet, thus showing that methyl groups are the most abundant surface intermediate. The CH_3–MA complexes, which block the methyl groups that are necessary for further reactions, cover only 8% of the surface, reflecting a very limited MA inhibition at these conditions. At the high pressure of 100 bar, the surface coverages of methyl, acetyl, and CH_3–MA are 21, 7, and 72%, respectively, at the reactor outlet, and the CH_3–MA coverage quickly grows to approximately 50% after about 1/6 of the catalyst mass. This result shows that under these conditions, the majority of the methyl groups is blocked as inactive CH_3–MA complexes and is not available for the reaction with CO. The surface coverage of acetyl is low (7%); however, it is 28% higher compared to the acetyl coverage at 10 bar.

Table 4 Parameters in the kinetic model

Parameter	Value
k_1	2.28×10^{-5} mol (mol Al)$^{-1}$ s^{-1} per bar
K_2	4.65 per bar
K_3	1.76

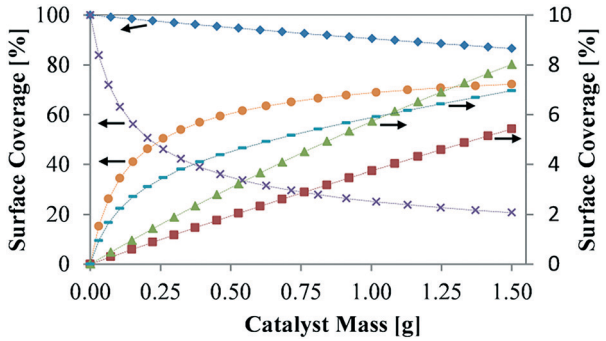

Fig. 10 Surface coverage profiles of methyl, acetyl, and methyl–MA complexes as a function of catalyst mass passed on the way through the bed. Coverages are calculated using the kinetic model. 10 bar, 2 vol% DME in CO, surface coverage of: (♦) methyl, (■) acetyl, (▲) methyl–MA complex. 100 bar, 2 vol% DME in CO, surface coverage of: (×) methyl, (–) acetyl, (●) CH_3–MA complex.

At differential reaction conditions, the MA pressure is negligible, and the rate expression [eqn (11)] reduces to:

$$r_{MA} \approx k_1 p_{CO} \quad (13)$$

Thus, our results are in good agreement with the previous experimental studies, in which the DME carbonylation over mordenite was studied at differential reaction conditions.[19,20] The rate expression [eqn (11)] proposed here is, however, also able to describe the reaction rates at high DME conversions and product concentrations, which are interesting from an industrial point of view.

4 Conclusions

Our detailed DFT study of the DME carbonylation over mordenite shows that the reaction of CO with a surface methyl group, the rate-limiting step in the reaction, is faster in the side pocket than in the main channel. The difference between the energy barriers for the rate limiting step at these two sites compares very well to the difference in adsorption energies of ammonia, supporting the hypothesis that the adsorption energy of ammonia is a good activity descriptor in solid acid catalysis. Also, we demonstrate that the reaction of DME with a surface acetyl group, a reaction in which MA is formed and the methyl group is regenerated, is possible entirely within the side pocket and is not rate-limiting. We have thus identified a path, where the entire reaction occurs favorably on a single site within the side pocket. Additionally, we show that MA and AcOH adsorb stronger than DME and MeOH on the Brønsted acid sites in the main channel where deactivation is thought to be focused,[22,25] which may help to explain why co-feeding of MA and AcOH inhibits the deactivation of mordenite during DME carbonylation.[50] In the side pocket, MA adsorbs on the Brønsted acid site with a similar strength as DME and MeOH. Consequently, the length of the initiation phase may depend of the MA pressure. Our experimental studies of the reaction kinetics are consistent with the theoretically determined mechanism and furthermore support the view that MA inhibits the reaction rate of MA synthesis. We hypothesize that this inhibition is due to sterical hinderance of the CO attack on the methyl groups within the side pockets. The kinetic model that we have developed for the steady-state phase of the reaction includes the effect of MA inhibition and provides a good description of the experimental data over a wide range of pressures and DME conversion levels.

Remaining challenges in a theoretical description of DME carbonylation

The Gibbs free energy diagram for the reaction (Fig. 11) indicates that there are still open questions concerning this reaction, as our current estimate of the entropic contribution makes the formation of MA from acetyl prohibitively difficult in the 8-MR, and since the available experimental data, if interpreted correctly, suggests the 8-MR as the focal point of the reaction.[26] However, it may also be added that this interpretation of the experimental data has been contested.[51]

The present work represents a breakthrough in terms of identifying a site in the 8-MR where both steps of the reaction mechanism (carbonylation and reaction between acetyl and DME) can occur with favorable energetics (Fig. 4), in agreement with the present interpretation of the experimental results. However, as noted, it is at present unclear, if the entropic contribution is prohibitive for the occurrence of the second step in the 8-MR. Molecular dynamics calculations could possibly yield a more accurate estimate of the entropies but this is outside the scope of our work.

In previous theoretical work the second step of the mechanism has been observed to occur with a prohibitively high

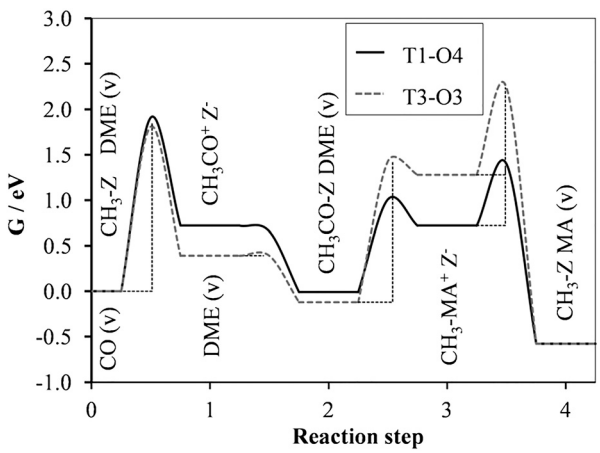

Fig. 11 Minimum Gibbs free energy path for formation of MA within the 12-MR on T1-O4 and the 8-MR on T3-O3 on mordenite (438 K, 10 bar CO, 0.2 bar DME, 0.02 bar MA). Reaction steps: 0: CO and DME in vacuum, methyl group on the zeolite; 1: acetyl carbocation, DME in vacuum and negatively charged zeolite; 2: acetyl group on zeolite, DME in vacuum; 3: CH_3–MA cation and negatively charged zeolite; 4: MA in vacuum, methyl group on zeolite. Full line: reaction steps in the main channel (T1-O4); dotted line: reaction steps in the side pocket (T3-O3).

barrier in the 8-MR, even in terms of the energies before consideration of the entropic contributions. To harmonize this disparity between experiments and theory Boronat *et al.* instead hypothesized a mechanism mediated by water, which is always present in small amounts due to the inevitable coke forming side-reactions.[29] This would allow the MA formation to occur in the 8-MR by an easier reaction between acetyl and CH_3OH:

$$H_2O + [SiO(CH_3)Al] \rightleftharpoons [SiO(H)Al] + CH_3OH \quad (14)$$

$$CH_3OH + [SiO(CH_3CO)Al] \rightarrow [SiO(H)Al] + CH_3COOCH_3 \quad (15)$$

$$CH_3OCH_3 + 2[SiO(H)Al] \rightleftharpoons 2[SiO(CH_3)Al] + H_2O \quad (16)$$

This mechanism would reconcile the disparities between theory and the interpretation of the experiments. Since the mechanism involves H-Z sites, also during the steady-state phase, this mechanism would also offer a straightforward explanation of the inhibition by MA from the strong adsorption of MA on H-Z sites (Table 2). However, the very low concentrations of methanol leaving the reactor at steady-state and the observation of inhibition by water added to the feed are on the other hand arguments against this mechanism.[19,20] A number of open questions thus remain for future theoretical and experimental studies of the DME carbonylation.

Appendix A

In this section we calculate the effectiveness factor for the catalyst particles used in this study. We only consider the effect of DME diffusion on the reaction rate because the concentration of CO, the other reactant, was very high in the reactant mixture in all experiments (at least 98 vol%). Consequently, the diffusion of CO is unlikely to be rate-limiting. The generalized Thiele modulus (φ) and the effectiveness factor (η) are calculated as described by Froment and Bischoff.[52]

The effectiveness factor (η) is calculated as [eqn (A.1)]:

$$\eta = \frac{3}{\varphi}\left(\frac{1}{\tanh\varphi} - \frac{1}{\varphi}\right) \quad (A.1)$$

The generalized Thiele modulus (φ) for a spherical particle and a zero order reaction is calculated using equation [eqn (A.2)]:

$$\varphi = \frac{R}{3}\cdot\sqrt{\frac{1}{2}\cdot\frac{k\cdot\rho}{C_{DME,s}\cdot D_{eff}}} \quad (A.2)$$

where R is the particle radius, k is the pseudo zero order rate constant for conversion of DME ($k = k_1{\cdot}P_{CO,s}$) under conditions with no MA present, ρ is the particle density, $C_{DME,s}$ and $P_{CO,s}$ are the concentration of DME and the partial pressure of CO at the particle surface (assumed the same as in the bulk), and D_{eff} is the effective diffusivity, which is calculated as:

$$D_{eff} = \frac{D_{12}\cdot\phi_p}{\tau} \quad (A.3)$$

where D_{12} is the binary diffusion coefficient, ϕ_p is the particle porosity and τ is the tortuosity. D_{12} for the diffusion of DME in CO is 2.29×10^{-3} cm^2 s^{-1} (438 K, 100 bar), calculated using the method of Brokaw for polar gases and Lennard-Jones potentials.[53,54] The parameter values used in the calculations are: particle radius R = 93.8 μm (mean of the sieve range used), rate constant $k = k_1{\cdot}P_{CO,s} = 3.18 \times 10^{-6}$ mol g^{-1} s^{-1} (the highest rate constant, k_1, in the kinetic model), the pressure of 100 bar (the highest reaction pressure), particle density ρ = 1.09 g cm^{-3}, concentration of DME $c_{DME,s} = 5.49 \times 10^{-5}$ mol cm^{-3} (2 bar, 438 K), porosity ϕ_p = 0.36 and tortuosity τ = 5.6.[55] The generalized Thiele modulus and the effectiveness factor are 4.59×10^{-3} and 1.00, respectively. Thus, the reaction is not limited by the diffusion.

Appendix B

As already discussed in the article, carbonylation of DME to MA over mordenite begins with an induction phase, in which the reaction rate of MA synthesis increases to a maximum, followed by a gradual loss in MA production, due to catalyst deactivation (Fig. 12). For kinetic modeling of the steady state reaction rate, a representative rate needs to be extracted from the measurements, and here two options are considered: namely 1) the maximum reaction rate reached during an experiment, or 2) an extrapolation of the measured activity to time 0 (assuming a constant deactivation rate throughout the entire experiment, see Fig. 12). In this work we have chosen to use option 1) because, even though the deactivation rate appears to be constant in Fig. 12, the chemical environment in the catalyst, such as the concentration of water and methanol is not the same during the induction phase and the period after maximal activity has been reached. Thus, the assumption of a constant deactivation rate throughout the experiment may not be valid. The choice of one or the other option will only lead to minor quantitative differences in the obtained kinetics. Although the rates extrapolated back to time 0 are higher than the peak rates, the relative dependence on the reaction conditions are similar for the two measures of activity (Fig. 12).

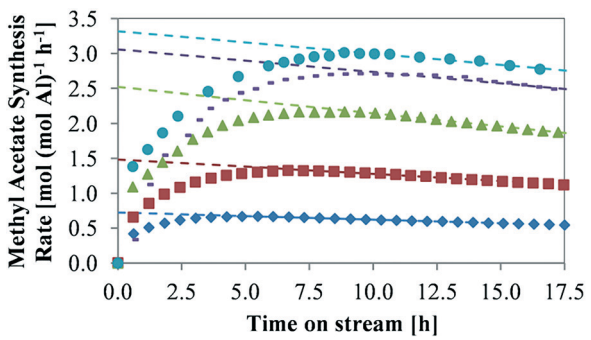

Fig. 12 MA synthesis rate as a function of time on stream (2 vol% DME in CO, 1.5 g catalyst): (♦) 10 bar, (■) 25 bar, (▲) 50 bar, (–) 80 bar, (●) 100 bar.

Appendix C

Table 5 Calculated frequencies of the reaction intermediates and transition states in formation of MA within the 12-MR on T1-O4 and the 8-MR on T3-O3 on mordenite. Reaction steps: 0: CO and DME in vacuum, methyl group on the zeolite; 1: acetyl carbocation, DME in vacuum and negatively charged zeolite; 2: acetyl group on zeolite, DME in vacuum; 3: CH_3–MA cation and negatively charged zeolite; 4: MA in vacuum, methyl group on zeolite

Reaction step	T1-O4 / cm^{-1}	T3-O3 / cm^{-1}
0 CO(v)	2157	
DME(v)	195, 252, 415, 900, 1082, 1143, 1153, 1172, 1243, 1439, 1460, 1468,	1472, 1481, 1494, 2927, 2940, 2976, 2980, 3075, 3077
CH_3–Z	20, 107, 253, 654, 1137, 1155, 1451, 1466, 1491, 3030, 3115, 3158	60, 155, 283, 647, 1129, 1156, 1449, 1475, 1486, 3041, 3132, 3158
0 → 1	476i, 36i, 119, 165, 167, 191, 214, 326, 358, 1066, 1096, 1206, 1365, 1388, 2191, 3025, 3222, 3277	490i, 43, 93, 105, 117, 140, 214, 345, 351, 1089, 1129, 1210, 1369, 1387, 2174, 3065, 3248, 3290
1	68i, 124, 125, 137, 195, 317, 423, 481, 951, 994, 1007, 1311, 1335, 1354, 2070, 2286, 2998, 3055	82, 126, 175, 187, 210, 339, 423, 463, 970, 1002, 1020, 1347, 1358, 1378, 2240, 2602, 2801, 3038
1 → 2	113i, 93i, 106, 109, 177, 320, 432, 484, 928, 981, 1005, 1253, 1306, 1314, 1997, 2246, 2985, 3040	69i, 51, 71, 118, 173, 292, 368, 403, 931, 1011, 1014, 1326, 1356, 1387, 2260, 2841, 2876, 3038
2	52i, 42, 116, 142, 280, 377, 537, 589, 963, 1038, 1097, 1386, 1435, 1460, 1880, 3008, 3094, 3142	42i, 101, 165, 186, 281, 348, 536, 575, 962, 1048, 1095, 1381, 1443, 1459, 1881, 3032, 3103, 3150
2 → 3	64i, 39i, 64, 75, 85, 95, 117, 138, 177, 187, 211, 229, 278, 375, 437, 510, 519, 780, 931, 949, 1013, 1054, 1129, 1142, 1177, 1243, 1356, 1422, 1432, 1438, 1455, 1463, 1469, 1472, 1480, 2048, 2951, 3014, 3018, 3030, 3111, 3117, 3138, 3139, 3174	129i, 32i, 67, 104, 124, 127, 146, 169, 197, 211, 239, 250, 271, 320, 337, 378, 444, 887, 906, 998, 1011, 1058, 1132, 1161, 1164, 1236, 1342, 1389, 1396, 1445, 1471, 1479, 1486, 1496, 1531, 2275, 2977, 2994, 3016, 3060, 3083, 3095, 3161, 3181, 3196
3	105i, 62i, 26i, 49, 79, 109, 122, 163, 189, 203, 251, 263, 290, 357, 442, 497, 509, 765, 926, 972, 1015, 1050, 1118, 1136, 1163, 1234, 1362, 1427, 1429, 1438, 1460, 1462, 1468, 1479, 1483, 2031, 2911, 3003, 3018, 3045, 3100, 3105, 3114, 3142, 3143	91, 108, 117, 119, 131, 153, 176, 202, 207, 276, 326, 339, 365, 406, 463, 531, 555, 752, 908, 989, 1040, 1075, 1141, 1148, 1181, 1246, 1386, 1439, 1447, 1453, 1470, 1473, 1486, 1490, 1498, 1957, 2969, 3074, 3089, 3099, 3172, 3187, 3246, 3254, 3279
3 → 4	342i, 91i, 15, 85, 97, 115, 125, 148, 163, 170, 194, 284, 298, 362, 439, 563, 614, 654, 898, 986, 1021, 1038, 1091, 1103, 1151, 1176, 1265, 1378, 1386, 1403, 1441, 1449, 1458, 1460, 1467, 1854, 3001, 3018, 3072, 3106, 3108, 3114, 3143, 3294, 3314	391i, 61, 114, 167, 168, 173, 183, 198, 249, 271, 307, 336, 356, 387, 459, 583, 617, 714, 889, 986, 1042, 1055, 1118, 1141, 1166, 1171, 1265, 1384, 1392, 1406, 1448, 1467, 1476, 1485, 1497, 1817, 3037, 3093, 3128, 3150, 3188, 3208, 3225, 3332, 3391
4 MA(v)	105, 155, 171, 286, 423, 588, 630, 819, 968, 1026, 1040, 1154, 1182, 1214, 1373, 1446, 1458, 1465, 1466, 1478, 1749, 3024, 3024, 3090, 3099, 3125, 3127	

Acknowledgements

The project is financed by the Technical University of Denmark (DTU) and the Catalysis for Sustainable Energy research initiative (CASE), funded by the Danish Ministry of Science, Technology and Innovation. Felix Studt gratefully acknowledges the support from the U.S. Department of Energy, Office of Science, Office of Basic Energy Sciences to the SUNCAT Center for Interface Science and Catalysis.

References

1 J. L. Keller, *Hydrocarbon Process.*, 1979, **58**, 127–138.
2 I. Wender, *Fuel Process. Technol.*, 1996, **48**, 189–297.
3 R. G. Herman, *Catal. Today*, 2000, **55**, 233–245.
4 M. M. Bhasin, W. J. Bartley, P. C. Ellgen and T. P. Wilson, *J. Catal.*, 1978, **54**, 120–128.
5 M. Ichikawa, *Bull. Chem. Soc. Jpn.*, 1978, **51**, 2273–2277.
6 P. Courty, D. Durand, E. Freund and A. Sugier, *J. Mol. Catal.*, 1982, **17**, 241–254.
7 K. J. Smith and R. B. Anderson, *Can. J. Chem. Eng.*, 1983, **61**, 40–45.
8 J. G. Nunan, C. E. Bogdan, K. Klier, K. J. Smith, C. W. Young and R. G. Herman, *J. Catal.*, 1989, **116**, 195–221.
9 E. Tronconi, L. Lietti, P. Forzatti and I. Pasquon, *Appl. Catal.*, 1989, **47**, 317–333.
10 P. Courty, P. Chaumette, C. Raimbault and P. Travers, *Rev. Inst. Fr. Pet.*, 1990, **45**, 561–578.
11 J. A. Dalmon, P. Chaumette and C. Mirodatos, *Catal. Today*, 1992, **15**, 101–127.
12 J. M. Christensen, P. M. Mortensen, R. Trane, P. A. Jensen and A. D. Jensen, *Appl. Catal., A*, 2009, **366**, 29–43.
13 J. M. Christensen, P. A. Jensen, N. C. Schiodt and A. D. Jensen, *ChemCatChem*, 2010, **2**, 523–526.
14 J. M. Christensen, P. A. Jensen and A. D. Jensen, *Ind. Eng. Chem. Res.*, 2011, **50**, 7949–7963.
15 X. San, Y. Zhang, W. Shen and N. Tsubaki, *Energy Fuels*, 2009, **23**, 2843–2844.
16 X. Li, X. San, Y. Zhang, T. Ichii, M. Meng, Y. Tan and N. Tsubaki, *ChemSusChem*, 2010, **3**, 1192–1199.

17 Y. Zhang, X. San, N. Tsubaki, Y. Tan and J. Chen, *Ind. Eng. Chem. Res.*, 2010, **49**, 5485–5488.
18 P. Haro, P. Ollero, A. L. V. Perales and C. R. Valle, *Energy*, 2012, **44**, 891–901.
19 P. Cheung, A. Bhan, G. J. Sunley and E. Iglesia, *Angew. Chem., Int. Ed.*, 2006, **45**, 1617–1620.
20 P. Cheung, A. Bhan, G. J. Sunley, D. J. Law and E. Iglesia, *J. Catal.*, 2007, **245**, 110–123.
21 J. Liu, H. Xue, X. Huang, Y. Li and W. Shen, *Catal. Lett.*, 2010, **139**, 33–37.
22 J. L. Liu, H. F. Xue, X. M. Huang, P. H. Wu, S. J. Huang, S. B. Liu and W. J. Shen, *Chin. J. Catal.*, 2010, **31**, 729–738.
23 H. F. Xue, X. M. Huang, E. Ditzel, E. S. Zhan, M. Ma and W. J. Shen, *Ind. Eng. Chem. Res.*, 2013, **52**, 11510–11515.
24 H. F. Xue, X. M. Huang, E. Ditzel, E. S. Zhan, M. Ma and W. J. Shen, *Chin. J. Catal.*, 2013, **34**, 1496–1503.
25 H. F. Xue, X. M. Huang, E. S. Zhan, M. Ma and W. J. Shen, *Catal. Commun.*, 2013, **37**, 75–79.
26 A. Bhan, A. D. Allian, G. J. Sunley, D. J. Law and E. Iglesia, *J. Am. Chem. Soc.*, 2007, **129**, 4919–4924.
27 B. Li, J. Xu, B. Han, X. Wang, G. Qi, Z. Zhang, C. Wang and F. Deng, *J. Phys. Chem. C*, 2013, **117**, 5840–5847.
28 M. Boronat, C. Martinez-Sanchez, D. Law and A. Corma, *J. Am. Chem. Soc.*, 2008, **130**, 16316–16323.
29 M. Boronat, C. Martinez and A. Corma, *Phys. Chem. Chem. Phys.*, 2011, **13**, 2603–2612.
30 J. J. Mortensen, L. B. Hansen and K. W. Jacobsen, *Phys. Rev. B: Condens. Matter Mater. Phys.*, 2005, **71**, 035109–035120.
31 J. Enkovaara, C. Rostgaard, J. J. Mortensen, J. Chen, M. Dulak, L. Ferrighi, J. Gavnholt, C. Glinsvad, V. Haikola, H. A. Hansen, H. H. Kristoffersen, M. Kuisma, A. H. Larsen, L. Lehtovaara, M. Ljungberg, O. Lopez-Acevedo, P. G. Moses, J. Ojanen, T. Olsen, V. Petzold, N. A. Romero, J. Stausholm-Moller, M. Strange, G. A. Tritsaris, M. Vanin, M. Walter, B. Hammer, H. Hakkinen, G. K. H. Madsen, R. M. Nieminen, J. K. Norskov, M. Puska, T. T. Rantala, J. Schiotz, K. S. Thygesen and K. W. Jacobsen, *J. Phys.: Condens. Matter*, 2010, **22**, 253202–253226.
32 S. R. Bahn and K. W. Jacobsen, *Comput. Sci. Eng.*, 2002, **4**, 56–66.
33 H. J. Monkhorst and J. D. Pack, *Phys. Rev. B: Solid State*, 1976, **13**, 5188–5192.
34 J. Wellendorff, K. T. Lundgaard, A. Mogelhoj, V. Petzold, D. D. Landis, J. K. Norskov, T. Bligaard and K. W. Jacobsen, *Phys. Rev. B: Condens. Matter Mater. Phys.*, 2012, **85**, 235149–235172.
35 A. Alberti, P. Davoli and G. Vezzalini, *Z. Kristallogr.*, 1986, **175**, 249–256.
36 C. G. Broyden, *Math. Comput.*, 1970, **24**, 365–382.
37 R. Fletcher, *Comput. J.*, 1970, **13**, 317–322.
38 D. Goldfarb, *Math. Comput.*, 1970, **24**, 23–26.
39 D. F. Shanno, *Math. Comput.*, 1970, **24**, 647–656.
40 G. Henkelman, B. P. Uberuaga and H. Jonsson, *J. Chem. Phys.*, 2000, **113**, 9901–9904.
41 E. Bitzek, P. Koskinen, F. Gaehler, M. Moseler and P. Gumbsch, *Phys. Rev. Lett.*, 2006, **97**, 170201–170205.
42 J. H. Noggle, *Physical Chemistry*, Little, Brown & Co., Boston, 1985.
43 H. G. Karge and V. Dondur, *J. Phys. Chem.*, 1990, **94**, 765–772.
44 O. Marie, P. Massiani and F. Thibault-Starzyk, *J. Phys. Chem. B*, 2004, **108**, 5073–5081.
45 A. Zecchina, G. Spoto and S. Bordiga, *Phys. Chem. Chem. Phys.*, 2005, **7**, 1627–1642.
46 D. B. Rasmussen, J. M. Christensen, B. Temel, F. Studt, P. G. Moses, J. Rossmeisl, A. Riisager and A. D. Jensen, *Angew. Chem., Int. Ed.*, 2015, **54**, 7261–7264.
47 P. G. Moses and J. K. Norskov, *ACS Catal.*, 2013, **3**, 735–745.
48 R. Y. Brogaard, C. M. Wang and F. Studt, *ACS Catal.*, 2014, **4**, 4504–4509.
49 C. M. Wang, R. Y. Brogaard, B. M. Weckhuysen, J. K. Norskov and F. Studt, *J. Phys. Chem. Lett.*, 2014, **5**, 1516–1521.
50 *US Pat.*, 8624054B2, 2014.
51 T. Bučko and J. Hafner, *J. Catal.*, 2015, **329**, 32–48.
52 G. F. Froment and K. B. Bischoff, *Chemical Reactor Analysis and Design*, John Wiley & Sons, New York, Chichester, Brisbane, Toronto, Singapore, 2nd edn, 1990.
53 R. S. Brokaw, *Ind. Eng. Chem. Process Des. Dev.*, 1969, **8**, 240–253.
54 B. E. Poling, J. M. Prausnitz and J. P. O'Connell, *The Properties of Gases and Liquids*, McGraw-Hill, New York, 5th edn, 2001.
55 A. K. Aboulgheit, M. F. Menoufy, A. K. Elmorsi and S. M. Abdelhamid, *Zeolites*, 1987, **7**, 353–359.